

Monitoring Drug-Induced Brain Activity Changes with Functional Ultrasound Imaging and Convolutional Neural Networks

Jared Deighton¹, Shan Zhong^{2,4}, Kofi Agyeman^{3,4}, Wooseong Choi⁵, Charles Liu^{4,5,6,7},
Darrin Lee^{4,5,6,7}, Vasileios Maroulas¹, Vasileios Christopoulos^{2,3,4,5,6}

¹Department of Mathematics, University of Tennessee, Knoxville, Knoxville, TN, USA;

²Neuroscience graduate program, University of California Riverside, Riverside, CA, USA;

³ Department of Bioengineering, University of California Riverside, Riverside, CA, USA;

⁴Alfred E.Mann Department of Biomedical Engineering, University of Southern California, Los Angeles, CA, USA;

⁵ Department of Neurological Surgery, Keck School of Medicine, University of Southern California, Los Angeles, CA, USA;

⁶ Neurorestoration Center, Keck School of Medicine, University of Southern California, Los Angeles, CA, USA;

⁷ Rancho Los Amigos National Rehabilitation Center, Downey, CA, USA;

* E-mail: Corresponding vchristo@usc.edu

Abstract

Functional ultrasound imaging (fUSI) is a cutting-edge technology that measures changes in cerebral blood volume (CBV) by detecting backscattered echoes from red blood cells moving within its field of view (FOV). It offers high spatiotemporal resolution and sensitivity, allowing for detailed visualization of cerebral blood flow dynamics. While fUSI has been utilized in preclinical drug development studies to explore the mechanisms of

action of various drugs targeting the central nervous system, many of these studies have primarily focused on predetermined regions of interest (ROIs). This focus may overlook relevant brain activity outside these specific areas, which could influence the results. To address this limitation, we combined convolutional neural networks (CNNs) with fUSI to comprehensively understand the pharmacokinetic process of Dizocilpine, also known as MK-801, a drug that blocks the N-Methyl-D-aspartate (NMDA) receptor in the central nervous system. CNN and class activation mapping (CAM) revealed the spatiotemporal effects of MK-801, which originated in the cortex and propagated to the hippocampus, demonstrating the ability to detect dynamic drug effects over time. Additionally, CNN and CAM assessed the impact of anesthesia on the spatiotemporal hemodynamics of the brain, revealing no distinct patterns between early and late stages. The integration of fUSI and CNN provides a powerful tool to gain insights into the spatiotemporal dynamics of drug action in the brain. This combination enables a comprehensive and unbiased assessment of drug effects on brain function, potentially accelerating the development of new therapies in neuropharmacological studies.

Introduction

Functional ultrasound imaging (fUSI) is an emerging hemodynamic-based neuroimaging technology that measures cerebral blood volume (CBV) changes by detecting backscattered echoes from red blood cells moving within its field of view (FOV) [1,2]. It provides a unique combination of large spatial coverage, high spatiotemporal resolution ($\sim 100 \mu\text{m}$ and $\sim 100 \text{ms}$) and sufficient sensitivity to detect slow blood flow changes (less than 1mm/s). The relative simplicity and portability of ultrasound scanners have allowed fUSI to be performed in a wide range of preclinical and clinical studies, providing minimally

invasive neural imaging in species ranging from mice to humans [3–8]. Among its various applications, fUSI has been employed in preclinical drug development to elucidate the mechanisms of action of drugs targeting the central nervous system. In particular, the mechanisms of various drugs, including anesthetics, cholinesterase agonists and antagonists, N-methyl-D-aspartate (NMDA) receptor antagonists, and selective norepinephrine reuptake inhibitors (SNRIs), have been investigated with the goal of better understanding their effects on brain function and vascular dynamics and accelerating the development of new drug therapies [9–12].

Despite the important contribution of these neuropharmacological studies, they predominantly focus on how drugs influence the hemodynamic signal in specific regions of interest (ROIs) and/or the functional connectivity between these regions. This approach inherently carries the risk of bias, as potentially relevant neural activity outside these predetermined areas may be ignored. Therefore, there is a clear and distinct need for developing advanced analytical methods with the capability to assess the dynamic effects of drugs on the brain without relying on a priori region specification. In the current study, we combine a convolutional neural network (CNN) approach with fUSI to elucidate the pharmacokinetics of Dizocilpine, also known as MK-801, in the brain. MK-801 is a potent and selective NMDA receptor antagonist that was initially employed as a pharmacological model of psychosis in rodents [13], and is still extensively utilized to model schizophrenia [14]. Saline injection is utilized as a vehicle control to establish a baseline comparison for evaluating the MK-801 drug effects in the brain. We also assess the impact of anesthesia on spatiotemporal dynamics of the brain activation throughout the experimental recordings using CNN. By combining CNN with Axiom-Based Grad-Class Activation Mapping (XGRAD-CAM) [15], which integrates principles of sensitivity and conservation, we are able to reveal the spatiotemporal effects of MK-801 and the influence

of anesthesia over time. The combination of fUSI and CNN provides a novel approach to explore the spatiotemporal patterns of drug action in the brain. This powerful methodology offers a comprehensive assessment of drug effects on brain function, facilitating the development of novel therapies in neuropharmacological studies without being limited to predefined ROIs.

Materials and methods

Animals

Twenty-three (23) 8-12 weeks-old male mice were utilized in this study (C57BL/6, Charles River Laboratories, Hollister, CA). All mice were group-housed, fed *ad libitum*, and maintained at a regular light-dark cycle of 12 hours. The animals were divided into two groups: MK-801 drug group (n=10) and saline vehicle control group (n=13).

Surgical Procedures

The mice were anesthetized using 5% isoflurane solution delivered in a mixture of oxygen and nitrous oxide (1:2 ratio) and then maintained at a constant isoflurane concentration of 1.5 - 2 % throughout the experiment. Body temperature was kept stable using an electric warming pad. The animals were head-fixed in a stereotaxic frame with ear bars to minimize head movement and reduce motion artifacts. A commercially available depilatory cream (Nair, Pharmapacks) was utilized to remove hair from the scalp followed by application of an echographic ultrasonic gel on the intact scalp-skin to enhance acoustic coupling during fUSI signal acquisition. All the experimental and surgical protocols were approved by the Institutional Animal Care and Use Committee of University of Southern

California (IACUC #21006).

Data Acquisition

Transcranial power Doppler (pD) images were obtained using the Iconeus One scanner (Iconeus, Paris, France). A 128-element linear array transducer probe with a 15.6 MHz center frequency and 0.1 mm pitch was placed on intact mice skull. The probe was fixed in a motorized system during the course of the experiment (Fig. 1A). Prior to recording, the target sagittal plane for imaging was determined by performing a 3-D whole-brain fUSI fast scan for each animal. The plane was then aligned with the standard Allen Mouse Common Coordinate Framework brain atlas using the specialized software provided with the Iconeus One system [16]. The details of fUSI parameters are described in [12]. Briefly, each image was constructed from 200 compounded frames, acquired at 500 Hz using 11 tilted plane waves (-10° to 10° , 2° increments). The pulse repetition frequency was 5.5 kHz, with continuous acquisition of 400 ms blocks of compounded images, separated by 600 ms intervals. This approach enables pD image acquisition with in-plane spatial resolution of $100\ \mu\text{m} \times 100\ \mu\text{m}$, slice thickness of $400\ \mu\text{m}$, FOV of 12.8 mm in width and 9.1 mm in depth, and an overall image-frame production rate of 1Hz (Fig. 1B). The fUSI data acquisition protocol consisted of 5 minutes of baseline recording, followed by intraperitoneal (i.p.) injection of either 0.2 ml of saline or MK-801 (1.5 mg/kg) at the 5 minutes mark and additional 55 minutes of recording, post-saline/MK-801 injection (Fig. 1C).

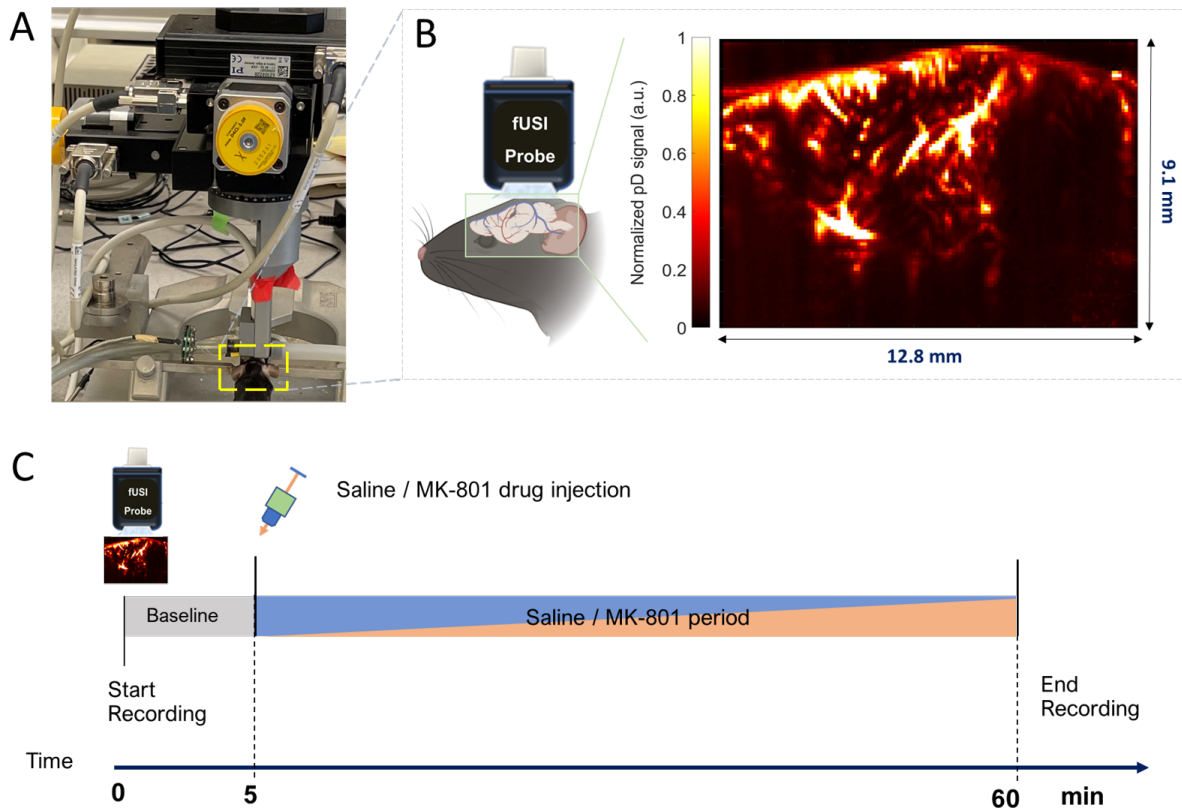


Figure 1. Experimental setup and fUSI acquisition. (A) fUSI motorized system setup for signal acquisition. (B) Power Doppler-based 2D vascular map image of a mouse brain in a sagittal plane. (C) Diagram of the experimental protocol for the 60 min of continuous fUSI acquisition. After 5 min, saline or 1.5 mg/kg MK-801 was intraperitoneally injected to the animals.

Data Pre-processing and Registration

We implemented the NoRMCorre motion correction method [17], combined with our in-house algorithms for filtering breathing and high-frequency signal to reduce noise. Specifically, we utilized a lowpass filter featuring a normalized passband frequency of 0.02 Hz and a stopband attenuation of 60 dB, which also offsets any delay caused by the filtering process, thereby eliminating high-frequency fluctuations.

Furthermore, we registered all the images to a common reference frame to ensure that

the CNN does not rely on the varying brain structures of different mice for image classification. We first identified the reference animal based on the imaging quality-i.e., we selected an animal with clear sub-cortical structures as the reference one. Then we computed the mean image of the first ten images beginning from the third minute of the baseline period to create a stable fixed image (reference image), in order to mitigate any potential variability that might arise from using a single image as a reference. We then employed the *Imregdeform* algorithm, which is a part of the Matlab Image Processing Toolbox (since 2022b). This algorithm utilizes a parametric approach for non-rigid image registration with total variation regularization. All images were aligned to the reference frame using the *Imregdeform* algorithm, which aids in simplifying subsequent data analysis.

CBV Change Calculation

CBV changes were quantified using the percent change in power Doppler signal ($\%pD$). For each ROI, the CBV changes were calculated relative to the baseline activity, which was defined as the mean pD signal intensity during the 5-minute baseline prior to MK-801/saline injection.

Training and Testing Data Sets

We employed a CNN model for two distinct classification tasks with fUSI data. Both tasks utilized a 10-fold cross-validation strategy for robust performance assessment.

For the MK-801 vs. saline classification task, in each iteration, data from 5 out of 10 MK-801 injected animals and 7 out of 13 saline-injected animals was randomly selected for training, while the remaining data was held out for testing. The model was trained on fUSI data from the last five minutes of post-injection recordings since our previous study

shows that the effects of MK-801 on brain activity become more potent over time [12]. Testing was conducted on the entire post-injection period using a one-minute sliding window.

For the early vs. late anesthesia stage classification task, only the saline-injected animals were used. The task compared fUSI data from the first five minutes post saline injection (early stage) vs. the last five minutes of recording (late stage). For each iteration, we randomly selected 7 animals from the 13 animals for training, and the remaining data was reserved for testing.

CNN Architecture

The CNN progressively reduces the spatial dimensions of the image input while increasing the depth of feature maps through four convolutional layers. After each layer, the model leverages the $ELU(\cdot)$ activation function, which is known to speed up learning and lead to higher classification accuracies by pushing the network’s mean activation toward zero [18]. The $ELU(\cdot)$ activation function is defined by

$$ELU(x) = \begin{cases} x & \text{if } x > 0 \\ \exp(x) - 1 & \text{if } x \leq 0 \end{cases}$$

Furthermore, the CNN ensures compatibility with class activation mapping through the use of an adaptive average pooling layer followed by a single linear layer. The linear layer outputs two features in correspondence with the binary classification task. Training details are summarized in Table 1.

Table 1. Hyperparameters used for training the networks.

Hyperparameter	Value
Batch size	32
Learning rate	1e-3
CNN nonlinearity	$ELU(\cdot)$
Optimizer	Adam [19]
CAM Technique	XGRAD-CAM [20]
Loss Function	Cross-entropy

Class Activation Mapping

Class activation mapping was performed using XGRAD-CAM [20] with a sliding time window of one minute. The localization map for a given input is computed as follows

$$L^{(c)}(x, y) = ReLU \left(\sum_k w_k^{(c)} A_k(x, y) \right) \quad (1)$$

with the coefficient $w_k^{(c)}$ being defined as

$$w_k^{(c)} = \sum_{i=1}^H \sum_{j=1}^W \left(\frac{\partial Y^{(c)}}{\partial A_k(i, j)} \cdot \frac{A_k(i, j)}{\sum_{m=1}^H \sum_{n=1}^W A_k(m, n)} \right) \quad (2)$$

where $A_k(x, y)$ is the activation of node k in the target layer of the model at position (x, y) and $Y^{(c)}$ is the model output score for class c before activation. Here, H and W are the height and width of the feature maps, respectively.

The target layer for this analysis was chosen to be the final convolutional layer, which contains higher-level feature representations and is commonly chosen for CAM [21].

The weights $w_k^{(c)}$ found in equation (2) were computed using the product of the gradient of the model’s raw score for the class (c) with respect to each activation and a normalization term. This encodes the importance of each activation in the final convolutional layer regarding the final classification decision for class (c). In our case, the final

convolutional layer produces 128 feature maps with height, $H = 16$, and width $W = 12$.

As described in (1), after calculating the weights for the given class and node, the weighted average was computed and the $ReLU(\cdot)$ activation function was applied to obtain the activation at each region. The result is a 12×16 activation map, corresponding to the dimensions of the feature maps from the final convolutional layer. To obtain a better picture for comparison with the initial image, the 12×16 image is upsampled to the original image size of 91×128 via bilinear interpolation.

We generated and analyzed activation maps for both classification tasks: MK-801 vs. saline and early vs. late stages of anesthesia. For each task, up-sampled activation maps were averaged per class to obtain summary maps. We then computed the difference between class summary maps to generate difference maps. After normalizing the difference maps to have values between 0 and 1, we applied an experimentally selected threshold, θ , to identify important regions for classification. The normalized difference class activation map $dCAM$ at each point (x, y) were computed as

$$\hat{D}(x, y) = L^{(A)}(x, y) - L^{(B)}(x, y)$$

$$dCAM(x, y) = \begin{cases} \hat{D}(x, y) & \text{if } \hat{D}(x, y) \geq \theta \\ 0 & \text{if } \hat{D}(x, y) < \theta \end{cases}$$

where $L^{(A)}$ and $L^{(B)}$ represent activation maps for the two classes being compared (MK-801 vs. saline, or early vs. late anesthesia stages, respectively). These difference maps highlight pixels that are most influential in distinguishing between conditions in each classification task.

Model performance

Model performance was assessed using 10-fold cross-validation for both classification tasks: MK-801 vs. saline and early vs. late stages of anesthesia. For each iteration, the model was trained on the designated training set and tested on the remaining test set, and a sliding window of one minute was utilized to analyze the model's performance over time. The adequacy of the model was evaluated using the following metrics:

- Accuracy: $(TP + TN) / (P + N)$.
- Precision: $TP / (TP + FP)$.
- Recall: $TPR = TP / P$.
- Area Under Curve (AUC): Area under the receiver operating characteristic (ROC), which is the plot of the true positive rate (TPR) against the false positive rate (FPR). FPR is defined as FN / P .
- F1-Score: Harmonic mean of precision and recall: $2TP / (2TP + FP + FN)$.

Where P and N represent the number of positive and negative instances, respectively, and TP, TN, FP, and FN denote true positives, true negatives, false positives, and false negatives. To reduce potential biases from individual training/testing set selections, we averaged evaluation metrics in each temporal window across all cross-validation iterations. The accuracy results of the CNN in predicting the effects of MK-801 and anesthesia on brain hemodynamics (i.e., correctly classifying between groups) are shown in Figure 3A and Figure 3B, respectively. The results for all metrics are presented in the Supplementary Materials.

Statistical Analysis

Paired t-test was performed to assess the significance of CBV changes between CAM-selected and non-CAM-selected ROIs. Statistical significance was set at $p \leq 0.05$. Statistical analysis was conducted using Matlab R2022b.

Results

CNN predicts MK-801 induced hemodynamic changes

To investigate the spatiotemporal effects of MK-801 injection on brain hemodynamics, we developed a CNN model using pD images recorded intracranially from anesthetized mice of two groups - one injected with MK-801, the other with saline as a vehicle for control. (Figure 2). Once collected the pD images, we implemented an advanced non-rigid image registration method, *Imregdeform*, to coherently align the image sets to a unified reference frame. We trained the CNN model using the pD images collected during the last 5 minutes of recording (55 minutes post-injection of either MK-801 or saline). We evaluated the ability of the model to distinguish between brain hemodynamic changes following MK-801 and saline injection and visualized the key brain regions involved in differentiating the two groups using the XGRAD-CAM algorithm to generate class activation maps (CAMs) [20]. The CAMs of the saline group were subtracted from those of the MK-801 group, generating dCAMs. These maps highlight the major differences in brain hemodynamic changes induced by MK-801 injection relative to saline. Regions that are active are hypothesized to represent areas where MK-801 elicited significant alterations in neural activity. For a detailed description of the CNN architecture, one may refer to the Materials and Methods Section.

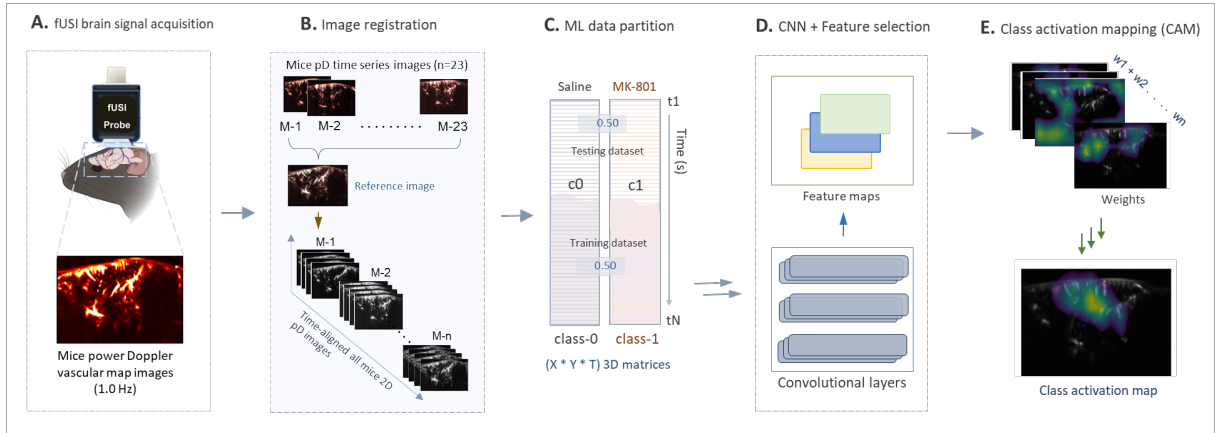


Figure 2. Flowchart of analysis pipeline. (A) fUSI mice brain signal acquisition. (B) Mice 2D power Doppler (pD) image time series alignment to a common reference image. (C) Data partitioning for CNN. (D) CNN and feature selection. (E) Class activation mapping.

We assessed the performance of the CNN model across successive 1-minute intervals spanning the 60-minute duration of the experiment, resulting in varying accuracy levels in response to the dynamic changes in brain activity following MK-801. Our hypothesis is that the CNN accuracy - the ability to dissociate between the two groups of animals based on the pD signal - is improved with time after the drug injection. Consistent with our hypothesis, we found that the CNN exhibited an accuracy near random chance level (57%, compared to 55% for true random) during the initial 5-minute baseline period before any injection was administered to the animals. This near-chance accuracy underscores the ability of the model to detect changes in brain activity resulting from the pharmacological intervention. As the temporal window progressed and the drug's effects intensified, the accuracy of the model improved, achieving a peak of $80.4 \pm 5.5\%$ (SD) at 35 minutes post-injection (Fig. 3 A).

Furthermore, to visualize how the key brain regions with differing hemodynamic responses to MK-801 versus saline injection evolve over time, we averaged the dCAMs across cross-validation folds for every 1-minute interval. This produced a temporal se-

quence that highlights the key regions exhibiting divergent hemodynamic activity over time. The averaged dCAMs across cross-validation folds from four distinct time points during the acquisition are shown in Fig. 4 A-D top panel (the complete video sequence is presented in the Supplementary Materials). The temporal evolution of the dCAMs reveal a progressive shift in the brain regions utilized by the CNN for classification, as captured by the dCAMs (CAM-selected ROIs). Initially, when the decoding accuracy was at chance level, the CAM-selected ROIs spanned across most of the brain, including pixels outside the brain. As time progressed, the CAM-selected ROIs gradually shrank, with the cortex and hippocampal regions emerging as the primary sites of divergence between the MK-801 and control groups. Concurrently, the pixels outside the brain disappeared from the CAM-selected ROIs.

This spatiotemporal pattern of MK-801’s effects aligns with previous findings, which showed that a single injection of MK-801 causes CBV reduction in the hippocampus and medial prefrontal cortex (mPFC) [12]. It may also suggest differential sensitivity of these regions to NMDA receptor blockade.

Moreover, we visualized the CBV changes in CAM-selected ROIs in MK-801 injected animals throughout the experiment. These CBV changes, expressed as percent change in power Doppler signal($\%pD$), provide a measure of cerebral blood volume alterations relative to the baseline over time. We computed the average CBV changes across the CAM-selected ROIs and compared with the average CBV changes of the non-CAM-selected ROIs across the recording sessions (Fig. 4 bottom panels). CAM-selected regions exhibited a significantly larger decrease in CBV compared to non-CAM-selected regions. Analysis of the last 5 minutes of recording revealed that CAM-selected regions showed a mean CBV change of -16.64% compared to -3.15% in non-CAM-selected regions (paired t-test, $p = 0.0003$, based on CAM map at $t = 50$ min post-injection). This

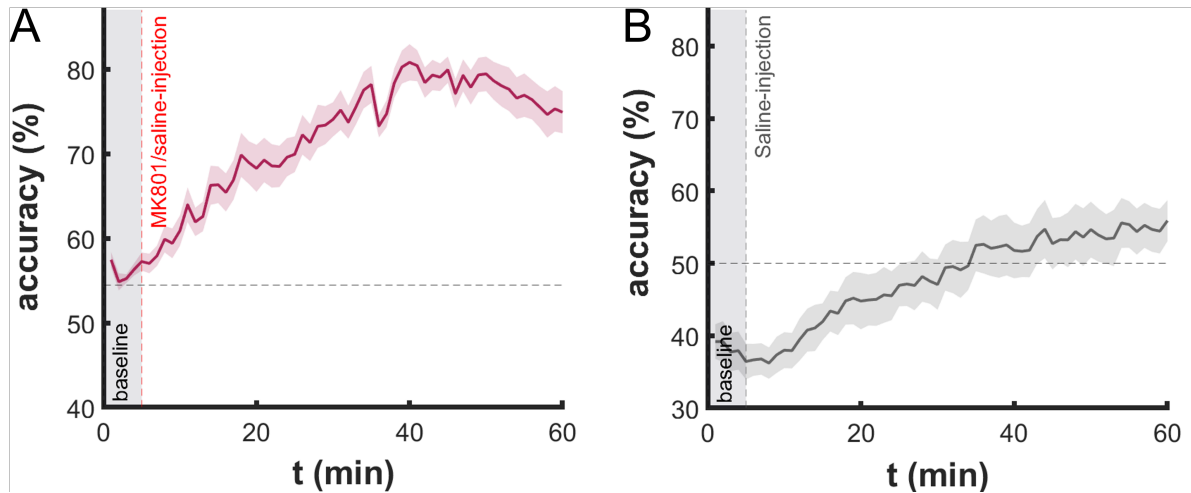


Figure 3. (A) CNN classification accuracy for distinguishing MK-801-induced hemodynamic changes from saline controls over time (the shaded area around the curve represents the standard error derived from averaging across animals.). Data was binned into one-minute time windows, on which the CNN was tested. (B) Same as panel A, but for distinguishing anesthesia-induced hemodynamic changes.

finding proves that as CBV progressively decreases following MK-801 injection, the most affected ROIs—i.e., the ones that best predict the differences between the two groups of animals—are predominantly localized in the cortex and hippocampus.

CNN predicts no significant anesthesia induced hemodynamic changes

We further applied the CNN-based methodology used for MK-801 analysis to the saline control group, in order to evaluate the hemodynamic effects induced by anesthesia. We trained the CNN on fUSI datasets from the first 5 minutes after saline injection and the last 5 minutes of recording, then tested its ability to discriminate between early and late stages of anesthesia.

The results showed that the CNN’s performance in predicting anesthesia-related hemo-

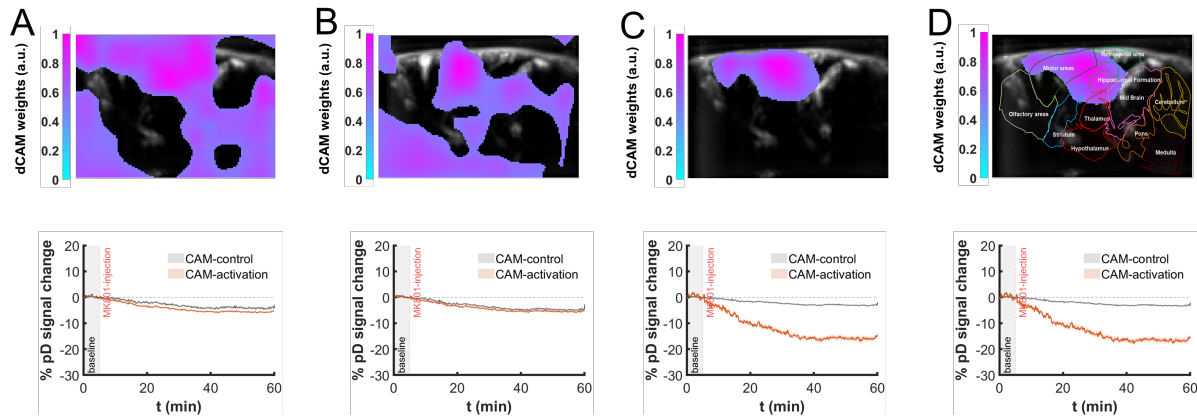


Figure 4. (A-D, top panel) Mean difference CAMs (dCAMs) at selected time windows (i.e., 1, 21, 33 and 50 min post-injection) following MK-801 injection. Brighter regions indicate areas of greater importance in CNN-based classification (threshold $\theta = 0.5$). (A-D, bottom panel) %*pD* (i.e., CBV) changes in the CAM-selected regions (orange curves) compared to non-selected control regions (grey curves).

dynamic changes was consistently around chance level throughout the recording period. (Fig. 3 B). The classification accuracy fluctuated around 49.87% ($\pm 6.73\%$ SD), and the highest accuracy achieved was 57.51% ($\pm 7.04\%$ SD) at 55 minutes post saline injection, which is only marginally above chance level. The dCAMs, generated by subtracting the initial five-minute post-saline CAMs from those of the final five minutes of recording, identified no consistent or significant ROIs related to anesthesia-induced changes (Fig. 5A-D, top panel shows that averaged dCAMs from four distinct time points). Unlike the MK-801 group, where specific brain regions emerged as important for classification over time, the difference CAMs for early vs. late stages of anesthesia in the saline group remained diffuse across the entire frame. Analysis of the last five minutes of CBV changes in the CAM-selected regions compared to non-CAM-selected regions revealed no significant differences (paired t-test, $p = 0.4601$, based on CAM map at $t = 50$ min post-injection) (Fig. 5A-D, bottom panel). The mean CBV changes change in CAM-selected regions was 0.34%, while in non-CAM-selected regions it was -0.24%. Collectively, these results

demonstrate that the CNN-based approach did not identify consistent or significant hemodynamic differences between the early and late stages of anesthesia in the saline group, likely due to the minimal effect of anesthesia on brain activity.

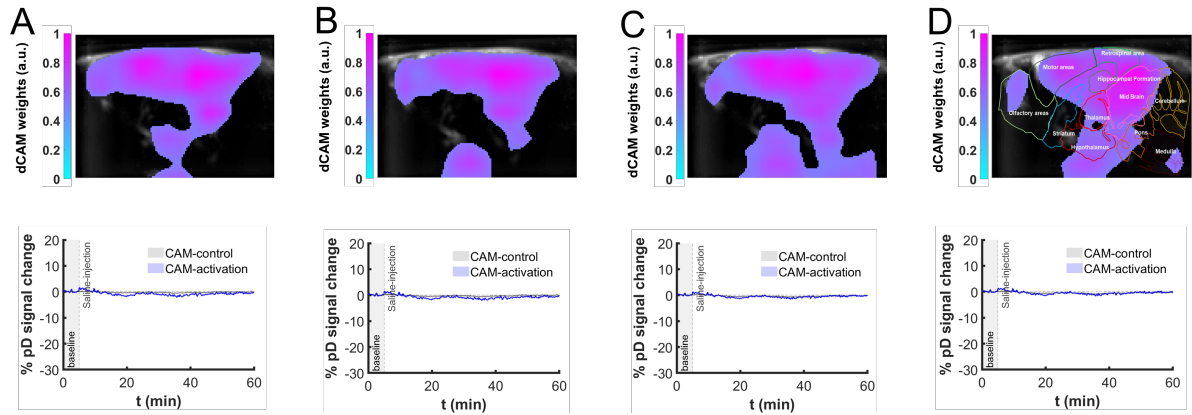


Figure 5. (A-D, top panel) Mean difference CAMs (dCAMs) at selected time windows (i.e., 1, 21, 33 and 50 min post-injection) following saline injection. Brighter regions indicate areas of greater importance in CNN-based classification (threshold $\theta = 0.5$). (A-D, bottom panel) Percentage CBV changes in the CAM-selected regions compared to non-CAM-selected regions. %*pD* (i.e., CBV) changes in the CAM-selected regions (blue curves) compared to non-selected control regions (grey curves).

Discussion

Functional ultrasound imaging (fUSI) is an emerging neuroimaging technology that measures CBV changes with high spatiotemporal resolution [1,2]. Its portability and minimal invasiveness have enabled wide-ranging preclinical and clinical applications, including neuropharmacological studies [9–12]. However, most fUSI studies in drug development focus on predetermined ROIs, potentially overlooking relevant neural activity elsewhere in the brain.

To overcome the limitations of traditional ROI-based analyses, we developed a novel approach that integrates convolutional neural networks (CNN) with functional ultrasound

imaging (fUSI) to evaluate the dynamic effects of drugs on the brain. The methodology integrates advanced non-rigid image registration techniques with deep learning analysis and class activation mapping, providing a powerful tool for investigating drug-induced changes in brain function with high spatial and temporal resolution. By combining fUSI with machine learning, we created a framework that not only detects but also localizes and tracks the progression of drug effects across brain regions, offering new insights into the complex dynamics of drug actions in the brain.

We demonstrated the effectiveness of this innovative method by investigating the pharmacokinetics of MK-801, a potent NMDA receptor antagonist commonly used in schizophrenia models [14]. Our findings showed that MK-801 administration leads to hemodynamic changes that is most prominent in the cortex and hippocampal areas. The CNN model exhibited high accuracy in classifying brain hemodynamic changes following MK-801 administration compared to saline-administered control animals. The performance of the model improved over time as the drug’s effect intensified, reliably detecting and differentiating drug-induced changes in brain activity. In contrast, the CNN’s performance in decoding anesthesia-related hemodynamic effects remained at chance level throughout the recording period, highlighting the specificity of our approach in detecting drug-induced changes in hemodynamic response, as the anesthesia-related effects are negligible.

While our study demonstrates the potential of combining fUSI with CNN-based techniques for investigating drug-induced changes in brain activity, there are several limitations. The current study focused on a single drug (MK-801) in a specific animal model. Future studies should explore the generalizability of our approach to other pharmacological agents or disease states in other animal models to further validate its utility and sensitivity. Moreover, while the results showed no significant effects of isoflurane anesthesia

on the brain hemodynamic signal, its use remains a potential limitation. Further research is needed to explore drug-induced effects in awake and freely moving animals. Additionally, although the CNN demonstrated high accuracy in classifying brain hemodynamic changes, the interpretability of CNN models remains a challenge. Future studies should focus on improving the interpretability of the CNN-based model and developing visualization techniques for better understanding the features that drive the model’s classification decisions. Finally, we trained the CNN model using data from the last five minutes of post-injection, since the effects of MK-801 on brain activity are well-documented to become more pronounced over time. If the drug’s pharmacokinetic profile is unknown, the model can be extended by applying a sliding window approach to train and test the CNN at various time intervals, starting from the moment of drug injection to the end of the recording.

Overall, the current study represents a significant step in applying deep learning techniques to fUSI data for investigating drug-induced effects on brain activity. By providing an unbiased approach for detecting and localizing the spatiotemporal effects of drugs in the brain, the proposed framework could improve the understanding of the complex dynamics of drug action in the brain and has the potential to accelerate drug and therapy development.

Acknowledgments

This work has been partially supported by the Army Research Laboratory Cooperative Agreement No W911NF2120186, the Army Research Office W911NF-21- 1-0094, the Keck School of Medicine Dean’s Pilot Funding Program (DL- PI), the National Institute of Mental Health (NIMH: 1K08MH121757-01A1), the USC Neurorestoration Center, and

the Marlan and Rosemary Bourns College of Engineering at the University of California Riverside through start-up funding.

Author Contributions

V.C. and V.M. conceived the study. W.C. acquire the data. S.Z. and K.A. performed data preprocessing. J.D. designed and implemented the convolutional neural network. J.D. performed class activation mapping. J.D., S.Z., and K.A. drafted the manuscript with contributions by C.L., D.L., V.M. and V.C. Finally, V.M. and V.C. revised and approved the manuscript.

Data Availability

The datasets generated and analyzed during the current study are available from the corresponding authors on reasonable request. The datasets cannot be used for commercial purposes, and we are unable to fulfill requests that would violate patient confidentiality, ethical guidelines, or patient consent agreements.

Code Availability

The code will be made available on GitHub upon publication.

References

1. Emilie Macé, Gabriel Montaldo, Ivan Cohen, Michel Baulac, Mathias Fink, and Mickael Tanter. Functional ultrasound imaging of the brain. *Nature methods*,

- 8(8):662–664, 2011.
2. Emilie Mace, Gabriel Montaldo, Bruno-Felix Osmanski, Ivan Cohen, Mathias Fink, and Mickael Tanter. Functional ultrasound imaging of the brain: theory and basic principles. *IEEE transactions on ultrasonics, ferroelectrics, and frequency control*, 60(3):492–506, 2013.
 3. BF Osmanski, C Martin, G Montaldo, P Laniéce, F Pain, M Tanter, and Gurden H. Functional ultrasound imaging reveals different odor-evoked patterns of vascular activity in the main olfactory bulb and the anterior piriform cortex. *NeuroImage*, 95:176–84, 2014.
 4. B.-F. Osmanski, S. Pezet, A. Ricobaraza, Z. Lenkei, and M. Tanter. Functional ultrasound imaging of intrinsic connectivity in the living rat brain with high spatiotemporal resolution. *Nature Communications*, 5(1):5023, 2014.
 5. M Imbault, D Chauvet, JL Gennisson, L Capelle, and Tanter M. Intraoperative functional ultrasound imaging of human brain activity. *Sci Rep.*, 7, 2017.
 6. C Demene, J Baranger, M Bernal, C Delanoe, S Auvin, V Biran, M Alison, J Mairesse, E Harribaud, M Pernot, M Tanter, and Baud O. Functional ultrasound imaging of brain activity in human newborns. *Sci Transl Med.*, 9, 2017.
 7. Sumner L Norman, David Maresca, Vassilios N Christopoulos, Whitney S Griggs, Charlie Demene, Mickael Tanter, Mikhail G Shapiro, and Richard A Andersen. Single-trial decoding of movement intentions using functional ultrasound neuroimaging. *Neuron*, 109(9):1554–1566, 2021.
 8. Whitney S Griggs, Sumner L Norman, Thomas Deffieux, Florian Segura, Bruno-Félix Osmanski, Geeling Chau, Vasileios Christopoulos, Charles Liu, Mickael Tan-

- ter, Mikhail G Shapiro, et al. Decoding motor plans using a closed-loop ultrasonic brain-machine interface. *Nature Neuroscience*, pages 1–12, 2023.
9. Claire Rabut, Jérémy Ferrier, Adrien Bertolo, Bruno Osmanski, Xavier Mousset, Sophie Pezet, Thomas Deffieux, Zsolt Lenkei, and Mickaël Tanter. Pharmaco-fus: Quantification of pharmacologically-induced dynamic changes in brain perfusion and connectivity by functional ultrasound imaging in awake mice. *Neuroimage*, 222:117231, 2020.
 10. B. Vidal, M. Droguerre, M. Valdebenito, L. Zimmer, M. Hamon, F. Mouthon, and M. Charvériat. Pharmaco-fus for characterizing drugs for alzheimer’s disease - the case of thn201, a drug combination of donepezil plus mefloquine. *Front Neurosci.*, 14:835, 2020.
 11. B. Vidal, M. Droguerre, L. Venet, M. Zimmer, M. Valdebenito, F. Mouthon, and M. Charvériat. Functional ultrasound imaging to study brain dynamics: Application of pharmaco-fus to atomoxetine. *Neuropharmacology*, 179, 2020.
 12. Lindsey M Crown, Kofi A Agyeman, Wooseong Choi, Nancy Zepeda, Ege Is-eri, Pooyan Pahlavan, Steven J Siegel, Charles Liu, Vasileios Christopoulos, and Darrin J Lee. Theta-frequency medial septal nucleus deep brain stimulation increases neurovascular activity in mk-801-treated mice. *Frontiers in Neuroscience*, 18:1372315, 2024.
 13. P Andiné, N Widermark, R Axelsson, G Nyberg, E Olofsson, U amd Mårtensson, and Sandberg M. Characterization of mk-801-induced behavior as a putative rat model of psychosis. *J Pharmacol Exp Ther*, 290:1393–408, 1999.

14. NC Zepeda, LM Crown, S Medvidovic, W Choi, M Sheth, M Bergosh, R Gifford, C Folz, P Lam, G Lu, R Featherstone, CY Liu, SJ Siegel, and Lee DJ. Frequency-specific medial septal nucleus deep brain stimulation improves spatial memory in mk-801-treated male rats. *Neurobiol Dis.*, 170, 2022.
15. Ruigang Fu, Qingyong Hu, Xiaohu Dong, Yulan Guo, Yinghui Gao, and Biao Li. Axiom-based grad-cam: Towards accurate visualization and explanation of cnns. *arXiv preprint arXiv:2008.02312*, 2020.
16. Quanxin Wang, Song-Lin Ding, Yang Li, Josh Royall, David Feng, Phil Lesnar, Nile Graddis, Maitham Naeemi, Benjamin Facer, Anh Ho, et al. The allen mouse brain common coordinate framework: a 3d reference atlas. *Cell*, 181(4):936–953, 2020.
17. E.A. Pnevmatikakis and A. Giovannucci. Normcorre: An online algorithm for piecewise rigid motion correction of calcium imaging data. *Journal of Neuroscience Methods*, 291:83–94, 2017.
18. Djork-Arné Clevert. Fast and accurate deep network learning by exponential linear units (elus). *arXiv preprint arXiv:1511.07289*, 2015.
19. Diederik P Kingma and Jimmy Ba. Adam: A method for stochastic optimization. *arXiv preprint arXiv:1412.6980*, 2014.
20. Fang Lu, Fa Wu, Peijun Hu, Zhiyi Peng, and Dexing Kong. Automatic 3d liver location and segmentation via convolutional neural network and graph cut. *International journal of computer assisted radiology and surgery*, 12:171–182, 2017.

21. Bolei Zhou, Aditya Khosla, Agata Lapedriza, Aude Oliva, and Antonio Torralba. Learning deep features for discriminative localization. In *Proceedings of the IEEE conference on computer vision and pattern recognition*, pages 2921–2929, 2016.